J Mater Sci (2008) 43:6938–6943
DOI 10.1007/s10853-008-2985-3

On the influence of carbon on secondary dendrite arm spacing in steel

Robert Pierer · Christian Bernhard

Received: 25 July 2008 / Accepted: 2 September 2008 / Published online: 23 September 2008

Abstract Solidification-related phenomena and the properties of the final product are strongly influenced by the developing dendritic microstructure, which is defined e.g. by the secondary dendrite arm spacing. In the past, different experimental set-ups were applied and subsequently the secondary dendrite arm spacing of certain steel grades was measured. However, it is difficult to compare the proposed relations based on either the local solidification time or the cooling rate, and they also vary over a wide range. Therefore, the present study systematically investigates the effect of carbon on the secondary dendrite arm spacing using in situ solidification experiments with accurately defined solidification conditions. The parameter K in the empirical equation $\lambda_2 = K \cdot t_f^{1/3}$ was determined as a function of carbon, using an iterative procedure to calculate the local solidification time and the measured secondary dendrite arm spacings. Furthermore, these results were discussed and compared with theoretical models from the literature.

Introduction

During the columnar dendritic solidification of steel phenomena such as hot tearing, microporosity formation and microsegregation may appear within the mushy zone. These phenomena, particularly microsegregation, depend on the dendritic microstructure, which is characterized by the primary λ_1 and secondary λ_2 dendrite arm spacing. Microsegregation strongly influences the formation of the liquid/solid two phase region (mushy zone) in terms of the characteristics of solid fraction f_S as a function of temperature T. Besides the microsegregation model and the model parameters such as the equilibrium partition coefficient k, the diffusion coefficient in the solid D_S and the liquidus slope of the solute elements m_L, the secondary dendrite arm spacing λ_2 and the local solidification time t_f strongly influence the results. In such calculations $\lambda_2/2$ is used as the back diffusion path and plays an important role [1].

Theoretical models [1–4] to calculate λ_2 are mainly based on the concept of Fick's law and the Gibbs-Thompson equation [5, 6]. The following theoretical equation can be derived for λ_2 as a function of the coarsening parameter M, the local solidification time t_f and a numerical (geometrical) factor B_0 [1–3]:

$$\lambda_2 = B_0 \cdot (M \cdot t_f)^{\frac{1}{3}} \tag{1}$$

where

$$M = -\frac{\Gamma \cdot D_L}{m_L \cdot (1-k)} \cdot A^{(i)} \quad (i = \text{model I, II, or III}) \tag{2}$$

In Eq. 2, Γ is the Gibbs-Thomson coefficient, D_L is the diffusion coefficient in the liquid, m_L the liquidus slope, and k is the equilibrium distribution coefficient. Depending on the different mechanisms of coarsening, the parameter $A^{(i)}$ results as follows:

$$A^{(i)} = \begin{cases} \frac{\ln(C_L/C_0)}{C_L - C_0} & \text{model I} \\ \frac{\ln(C_L/C_0)}{C_L - C_0} & \text{model II} \\ \frac{1}{C_0} \cdot \int_{0.1}^{f_S^*} \frac{df_S}{(1-f_S)^{k-1} \cdot f_S \cdot (1-\sqrt{f_S})} & \text{model III} \end{cases} \tag{3}$$

where C_L is the liquid and C_0 the initial concentration. In these models, the coarsening is considered as lateral

R. Pierer (✉) · C. Bernhard
Department of Metallurgy, CD Laboratory for Metallurgical Fundamentals of Continuous Casting Processes,
Franz Josef Str. 18, 8700 Leoben, Austria
e-mail: robert.pierer@mu-leoben.at

remelting of the minor arms (model I, $B_0 = 5.48$) [2], as remelting of the smaller arms from their tips towards their roots (model II, $B_0 = 5.04$) [1] and as lateral remelting of the minor arms involving the solid fraction during solidification and the consideration of the number and width of survival arms (model III, $B_0 = 1.89$) [3]. Mortensen [3] assumed in his study that $f_S^* = 0.93$, which is the solid fraction at which the eutectic forms and solidification ceases.

The local solidification time t_f in Eq. 1 is defined as the time where the temperature at a given location in a casting decreases from the liquidus to the nonequilibrium solidus [1]. However, these models apply to binary alloys and therefore Rappaz and Boettinger [7] extended model I to multicomponent alloys. In addition, Han et al. [8] expanded four models of isothermal coarsening of λ_2 to multicomponent alloys. Zhang et al. [9] for example developed a simple model by introducing the diffusion layer thickness and validated the calculated values using Al–Cu–Mg alloys. Nevertheless, in the case of steel only empirical relations of the form $\lambda_2 \sim \dot{T}^{-n}$ or $\lambda_2 \sim t_f^n$ were developed based on measured λ_2-values. However, for a given alloy, λ_2 mainly depends on the time from the onset of solidification, whereas the cooling conditions only show a minor effect [1]. Considering the development of λ_2 during solidification from the viewpoint of coarsening kinetics, the relation between λ_2 and t_f clearly is preferred:

$$\lambda_2 = K \cdot t_f^n \tag{4}$$

where K and n are used as parameters to fit the experimental data. In the literature, these parameters were mainly determined for certain steel grades, where different experiments and methods to determine solidification variables (e.g. t_f or $\dot{T}$) are used. Based on these λ_2-measurements some studies [10–13] proposed λ_2-relations, where the fitting parameters are defined as a function of steel composition. As a result, these equations lead to a large scatter of calculated, hardly comparable λ_2-values.

Therefore, the present study systematically investigates the influence of carbon on λ_2. Considering that the development of λ_2 follows a coarsening mechanism (i.e. $n = 1/3$), only K as a function of carbon is used as a fitting parameter. The experimental technique will be briefly described focusing on the calculation of t_f. A further important part of the present study represents the metallographic determination of λ_2 which will also be described in the next section. Based on Eq. 4, the parameter K is determined as a function of carbon and will be compared with the above described models I–III in section "Results and discussion".

Experimental procedure and simulation

Test arrangement

The experiment used to investigate the influence of carbon on λ_2 is the Submerged Split Chill Tensile test, a testing method with conditions very similar to those occurring in a continuous casting mould. The principle of this testing method has been explained in detail e.g. in [14] and is schematically illustrated in Fig. 1. It represents an in situ solidification experiment where a cylindrical test body is submerged into the liquid melt in an induction furnace. A steel shell solidifies around the test body resulting in a columnar grain structure perpendicular to the interface. The heat flux at the chill-shell interface is controlled via the thickness of the spray-coated zirconium oxide layer. In the present study, the coating thickness of the test body is 0.40 mm which results in a maximum heat flux of $\sim$1.7 MW/m^2 and a mean heat flux of $\sim$1.25 MW/m^2. The investigated carbon contents are 0.08, 0.12, 0.16, 0.30, 0.50, and 0.70 wt.% with a basic composition of $\sim$0.28 wt.% Si, $\sim$1.32 wt.% Mn, 0.007 wt.% P, and 0.007 wt.% S. According to this procedure, the solidification conditions can accurately be defined and described by a numerical analysis, which will be presented in section "Calculation of t_f".

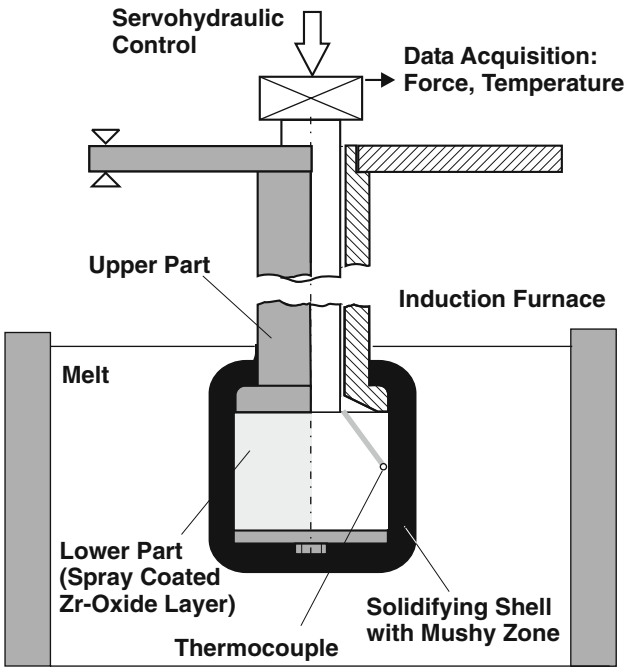

Fig. 1 Schematic illustration of the SSCT method: a steel shell solidifies around the cylindrical test body within the induction furnace

Metallographic determination of λ_2

The λ_2-values are measured at two samples per carbon content—positioned oppositely to each other—from the solidified specimens. The longitudinal sections (parallel to the dendritic growth direction) were polished and etched with a solution of 11 g CrO_3, 55 g NaOH, and 100 ml H_2O (distilled). These sections were captured by a digital image analysis system in the form of a mosaic, containing up to 50 single micrographs. Finally, the λ_2-values were measured at different distances from the chill-shell interface (position: 1, 3, 5, 7, and 9 mm). The corresponding t_f is calculated as described in the next section. The number of measurements is approximately 100 per position in a range of ±0.2 mm along the different distances. The above described procedure is illustrated in Fig. 2.

The following rules regarding the measurement of the secondary dendrite arm spacing were applied:

- Along primary grain boundaries (PGB), a stronger coarsening of the secondary dendrite arms takes place. This was quantified by Zhang and Singer [15] in terms of primary dendrite arm spacing of Ni-base alloys. These authors reported a value of approximately 1.5 for the ratio $\lambda_{1,PGB}/\lambda_1$. Unpublished results from our own measurements of carbon steels also show a value of approximately 1.5 for the $\lambda_{2,PGB}/\lambda_2$-ratio. Therefore, λ_2-measurements along PGB were avoided in the present study.
- Generally, the microstructure also includes secondary dendrite arms which were constricted in their growth by adjoining dendrite arms. As a result, measurements along the primary dendrite trunk lead to larger values than measurements at higher distances to the trunk. Therefore, it was tried to measure λ_2 at constant distances from the dendrite trunk.
- Secondary dendrite arms, which had already developed tertiary dendrite arms, were not considered in the measurements.
- Measurements of secondary dendrite arms very close to the dendrite tip result in lower values and thus, must also be avoided.

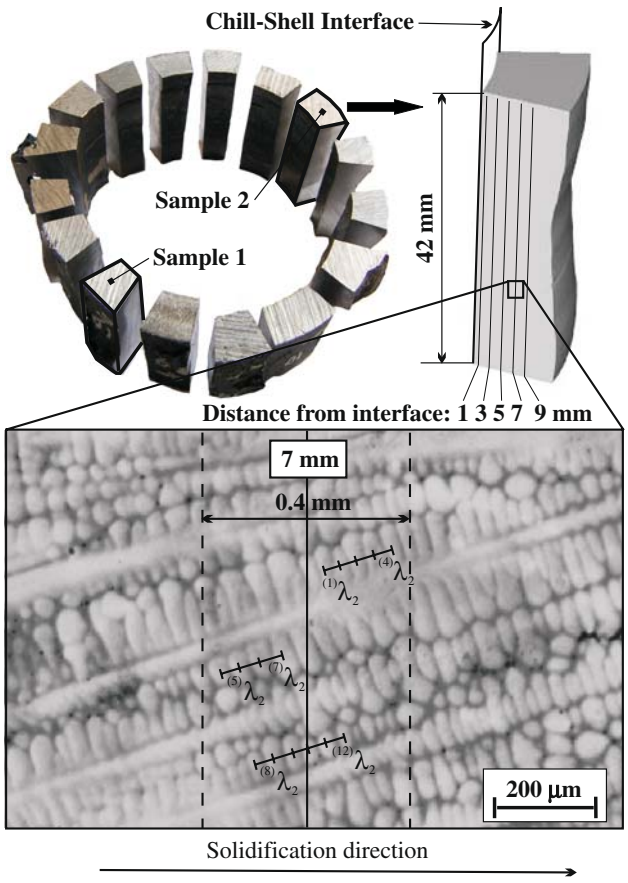

Fig. 2 Illustration of the metallographic procedure to determine λ_2 and a part of the micrograph at a distance of 7 mm from the interface for a 0.70 wt.% C steel

Calculation of t_f

In order to calculate t_f, a thermal analysis of the experiment is carried out by determining the enthalpy distribution between the chill surface and the inner side of the induction furnace using one-dimensional heat conduction. Due to the axisymmetric geometry of the test body, Eq. 5 is written in cylindrical coordinates:

$$\frac{\partial}{\partial t}(\rho \cdot H) = \frac{1}{r} \cdot \frac{\partial}{\partial r}\left(r \cdot k \cdot \frac{\partial T}{\partial r}\right) \tag{5}$$

where ρ is the temperature-dependent density, H denotes the enthalpy, k stands for the temperature-dependent thermal conductivity, r is the radius, T is the temperature, and t is the time. The enthalpy $H(T)$ is given by the following equation:

$$H(T) = \int_0^T c_P(T') \cdot \mathrm{d}T' + (1 - f_S) \cdot \Delta H_{LS} \tag{6}$$

where ΔH_{LS} is the latent heat and c_P is the specific heat capacity. The initial and boundary conditions are listed and defined in Fig. 3. The heat flux density q is calculated at the chill-shell interface by means of the temperature increase inside the test body—recorded in a defined distance from the chill-shell interface—using an inverse algorithm for the solution of Eq. 5. The calculation procedure is based on a maximum-a-posteriori method and is described in detail in [16].

The solution of Eq. 5 is achieved with the finite volume method, where the temperature-dependent parameters were

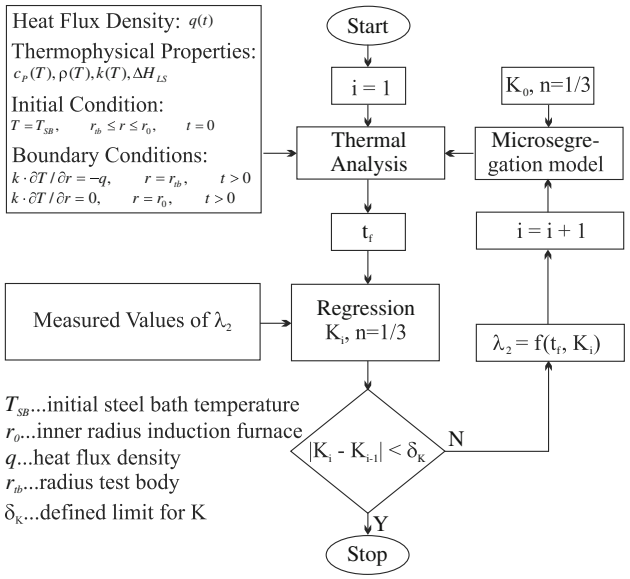

Fig. 3 Flow chart of the iterative procedure to determine the parameter K

taken from the software package IDS [17]. The thermal analysis also includes the microsegregation model according to Ueshima et al. [18]. An important input parameter in microsegregation calculations is Eq. 4. However, this relation influences the results of t_f. Therefore, an iterative procedure as illustrated in Fig. 3 is applied to determine K. Using the empirical relation $\lambda_2 = K \cdot t_f^{1/3}$, the calculated values of t_f and the measured values of λ_2 a nonlinear regression is carried out to determine K for each carbon content.

Results and discussion

A very large number of λ_2-values is available, because 100 λ_2-values were measured at each position from the chill-shell interface. Thus, the influence of possible measurement errors on the final result can be minimized. Furthermore, two samples per carbon content were investigated in order to even out possible differences in solidification conditions. This situation is representatively shown in Fig. 4 for the 0.50 wt.% C steel. The mean λ_2-values are illustrated as a function of the number of measurements. Furthermore, the results of the two samples ($\lambda_2^{(1)}$ and $\lambda_2^{(2)}$) are illustrated for each different position from the chill-shell interface. It can be seen very clearly that the measurement of 100 λ_2-values is absolutely adequate. Moreover, it seems that the consideration of more than 50 values do not significantly change the mean λ_2-value. Considering the results of sample 1 and sample 2 at the same position from the interface a very good correspondence was reached. The resulting λ_2-values of these

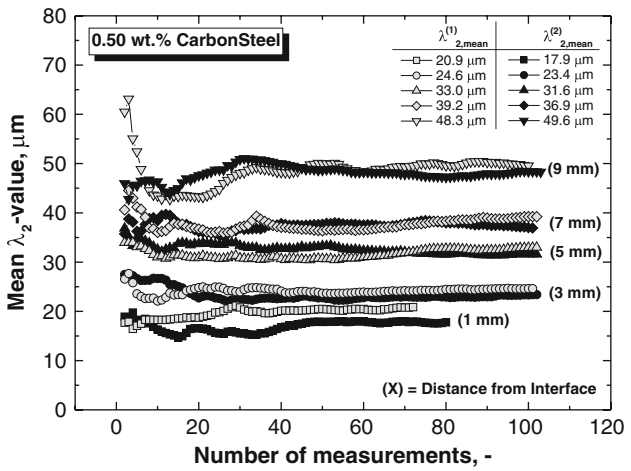

Fig. 4 Mean λ_2-values as a function of the number of measurements for the 0.5 wt.% carbon steel

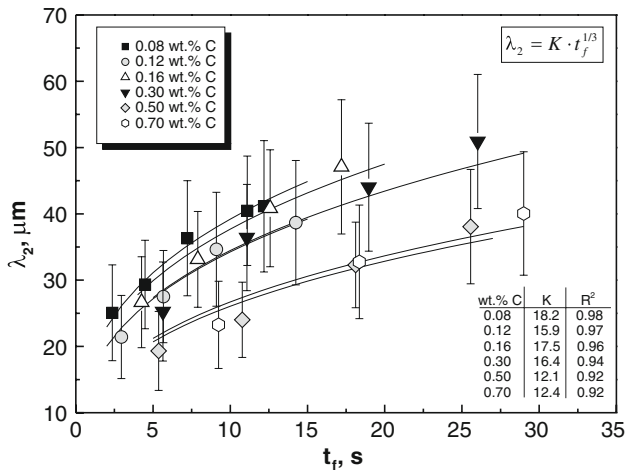

Fig. 5 Experimentally determined λ_2 as a function of t_f for different carbon contents together with the calculated curves using the empirical λ_2-equation

two samples are additionally listed in Fig. 4 for the 0.50 wt.% C steel.

In order to determine the parameter K in the empirical λ_2-equation, the mean value of the two samples is used. These values are summarized in Fig. 5 for all carbon contents as a function of the corresponding t_f. Additionally, the error bars in terms of standard deviation are illustrated. The extent of the scatter band can be explained by measurement errors and is also a result of the width of the considered measurement range along the different distances. However, it is in the same order of magnitude which is reported in the relevant literature [19].

Based on the illustrated λ_2-values in Fig. 5 and applying a nonlinear regression, the parameter K in Eq. 4 was determined for each carbon content. Therefore, the iterative procedure—illustrated in Fig. 3 and described

previously—was used. The resulting values of K are listed and the calculated curves are illustrated in Fig. 5. It can be seen that the trend of λ_2 can be described very well using Eq. 4. The results show that with increasing carbon content, K tends to decrease from approximately 18–12 when considering the theoretical value of $n = 1/3$. In the literature (e.g summarized in [19]), n and K of carbon steels range between 0.32–0.59 and 2.1–52, respectively. Considering a constant solidification time, the characteristics of K as a function of carbon content reflect also the influence of carbon on the secondary dendrite arm spacing. Hence, increasing the carbon content results in a decrease of λ_2. This behavior is e.g. in accordance with the empirical equation proposed by Miettinen [11] but does not agree with the empirical equation suggested by Cabrera-Marrero et al. [13], which predicts an increasing λ_2-value with increasing carbon content.

Due to the otherwise constant chemical composition, K as a function of the carbon content can be best approximated using an equation in the form of $a + b \cdot \mathrm{C}^{1/3}$. Thus, the secondary dendrite arm spacing for the investigated steel grades can be calculated using the following empirical λ_2-relation:

$$\lambda_2(\mu\mathrm{m}) = (23.7 - 13.1 \cdot \mathrm{wt.\%C}^{\frac{1}{3}}) \cdot t_\mathrm{f}^{\frac{1}{3}} \tag{7}$$

This equation is valid for carbon contents between 0.08 and 0.7 wt.% (basic composition: ~0.28 wt.% Si, ~1.32 wt.% Mn, 0.007 wt.% P and S) and a validity area of $15 \leq \lambda_2(\mu\mathrm{m}) \leq 50$.

In order to compare these results with theoretical approaches, the models according to Feurer and Wunderling (model I) [2], Kirkwood (model II) [1] and Mortenson (model III) [3] are applied. However, at steels with 0.12, 0.16, and 0.30 wt.% C it is clear that a peritectic transition takes place during solidification, which cannot be considered using Eq. 2. Hence, it is assumed that when the peritectic transition occurs (i.e. $f_\mathrm{S} = f_\mathrm{S}^{\delta-\gamma}$) the conditions change from δ to γ-Fe. Assuming further that $\frac{\mathrm{d}f_\mathrm{S}}{\mathrm{d}t} = \frac{1}{t_\mathrm{f}}$ [3] results in the following approximation of M

$$M^{(\mathrm{I,II})} = M_\delta \cdot f_\mathrm{S}^{\delta-\gamma} + M_\gamma \cdot (1 - f_\mathrm{S}^{\delta-\gamma}) \tag{8}$$

for model I and II, respectively. Please note that M in model I and II is equal, only the numerical factor B_0 differs in these two models. In the case of model III, the following equation is used to calculate the coarsening parameter M:

$$\begin{aligned} M^{(\mathrm{III})} = &- \frac{\Gamma \cdot D_\mathrm{L}}{m_{\mathrm{L},\delta} \cdot (1 - k_\delta)} \cdot A_\delta^{(\mathrm{III})} \\ &- \frac{\Gamma \cdot D_\mathrm{L}}{m_{\mathrm{L},\gamma} \cdot (1 - k_\gamma)} \cdot A_\gamma^{(\mathrm{III})} \end{aligned} \tag{9}$$

In the original work of Mortenson, the Scheil equation is used, since the model was validated for Al–Cu alloys. However, in the case of Fe–C (it is assumed that only carbon influences the coarsening process) it can be shown by calculating the Fourier number ($Fo = (D_\mathrm{L}$ or $D_\mathrm{S}) \cdot t_\mathrm{f}/L^2$) that the Lever rule is more appropriate. Replacing the Scheil equation by the Lever rule results in:

$$\begin{aligned} A_\delta^{(\mathrm{III})} &= 1/C_0 \cdot \int_{0.1}^{f_\mathrm{S}^{\delta-\gamma}} \frac{1 - f_\mathrm{S} \cdot (1 - k_\delta)}{f_\mathrm{S} \cdot (1 - \sqrt{f_\mathrm{S}})} \cdot \mathrm{d}f_\mathrm{S} \\ A_\gamma^{(\mathrm{III})} &= 1/C_0 \cdot \int_{f_\mathrm{S}^{\delta-\gamma}}^{1} \frac{1 - f_\mathrm{S} \cdot (1 - k_\gamma)}{f_\mathrm{S} \cdot (1 - \sqrt{f_\mathrm{S}})} \cdot \mathrm{d}f_\mathrm{S} \end{aligned} \tag{10}$$

Applying $f_\mathrm{S} = 0.1$ as the lower integration limit implies that the coarsening at f_S lower than 0.1 is ignored [3]. The solid fraction at which the peritectic transition occurs is calculated using the Lever rule and follows the procedure suggested by Cornelissen [20]. For a liquid phase carbon concentration lower than 0.5 wt.% δ-Fe develops, whereas at a carbon content over 0.5 wt.% an austenitic (γ-Fe) structure occurs. Therefore, Cornelissen assumes that only the carbon content controls the transition (other components do not effect the δ–γ transformation). Using the Lever rule and inserting 0.5 wt.% C as the liquid carbon concentration at which the transition occurs, $f_\mathrm{S}^{\delta-\gamma}$ can be calculated as follows:

$$f_\mathrm{S}^{\delta-\gamma} = \frac{0.5 - C_0}{0.5 \cdot (1 - k_\delta)} \tag{11}$$

The necessary liquid concentration C_L in model I and II is also calculated using the Lever rule and the Gibbs-Thomson coefficient Γ is calculated by IDS [17]. Using $k_\delta = 0.19$, $k_\gamma = 0.34$, $m_\mathrm{L},\delta = -82.7$, $m_\mathrm{L},\gamma = -60.9$ [18], and $D_\mathrm{L} = 7{\cdot}10^{-9} m^2/s$ [21], K can be calculated according to $K = B_0 \cdot M^{\frac{1}{3}}$ for each model and carbon content. The results are illustrated in Fig. 6 together with the K-values of the present study.

It can be seen that every theoretical model leads to decreasing K-values with increasing carbon content, very similar to the determined values of the present study. However, applying model I and II with the corresponding values of $B_0 = 5.48$ and 5.04, respectively, results in K-values clearly higher than the predicted values of the present study. In terms of λ_2 this difference in K results in approximately 1.3–1.6 times higher values than the measured λ_2-values. However, B_0 depends on the assumed geometry of the coarsening process and was viewed as approximate value [7]. Furthermore, due to the extreme simplification of the coarsening process in these models, the value and constancy of B_0 should not be overestimated [22]. Therefore, reducing this parameter to 3.36 and applying model I or II would result in K-values very similar to the values calculated using $K = 23.7 - 13.1\,\mathrm{wt.\%\,C}^{1/3}$

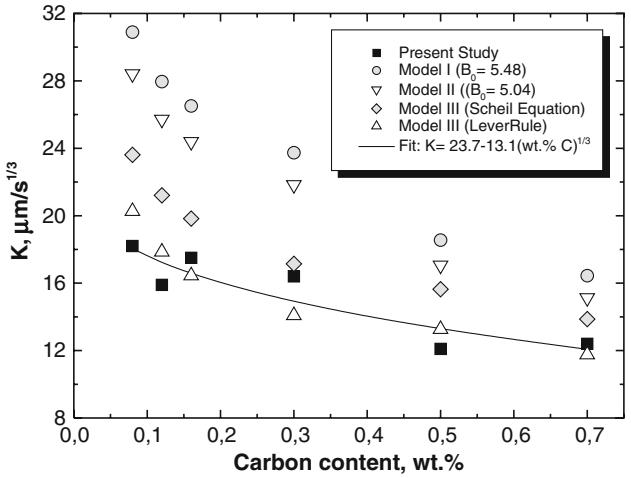

Fig. 6 *K*-values as a function of carbon content of the present study in comparison with calculated values using the three different models

(solid line in Fig. 6). Considering model III, the calculated *K*-values are higher when using the Scheil equation but correspond very well with the Lever rule. Therefore, it can be stated that under the conditions of the present study, the influence of carbon content on the secondary dendrite arm spacing can be best described using the modified model III.

Summary and conclusion

In the present study, the influence of carbon content on the secondary dendrite arm spacing was investigated. The carbon content varies between 0.08 and 0.70 wt.% with a basic steel composition of ~0.28 wt.% Si, ~1.32 wt.% Mn, 0.007 wt.% P and S. For each carbon content two samples were analyzed. The secondary dendrite arm spacing was determined at five different positions within the micrograph, each with 100 measurements. The corresponding local solidification time was calculated applying an iterative procedure of the thermal analysis. For each investigated carbon content it was shown that the measured values of the secondary dendrite arm spacing can be described by $\lambda_2 = K \cdot t_f^{1/3}$, where $K = 23.7 - 13.1\,\mathrm{wt.\%\,C}^{\frac{1}{3}}$. Considering the influence of carbon, it follows that with increasing carbon content the secondary dendrite arm spacing generally decreases for lower values of the local solidification time, whereas at higher values, a maximum is reached at 0.16 wt.% C. From the calculation results using the three different theoretical models of coarsening during solidification it can be concluded that model III leads to the best agreement with the measured secondary dendrite arm spacings of carbon steels. This model differs from model I and II by focusing on growing dendrite arms and the consideration of the effect of a finite volume solid fraction. However, due to the necessary integrations it is more complicated in handling compared to model I and II.

Acknowledgements The authors gratefully acknowledge Martina Hanel and Juergen Reiter for their support as well as the funding of this work by the Austrian Ministry for Economy and Labour in the frame of the Christian Doppler Laboratories.

References

1. Kirkwood DH (1985) Mater Sci Eng 73:L1
2. Feurer U, Wunderlin R (1977) Deutsche Gesellschaft f. Metallkunde
3. Mortensen A (1991) Metall Mater Trans 22A:569
4. Voorhees PW (1990) Metall Mater Trans 21A:27
5. Salas GB, Ramrez JV, Noguez MEA, Robert TN (1995) Scripta Metall Mater 32:295
6. Melo MLNM, Rizzo EMS, Santos RG (2005) J Mater Sci 40:1599
7. Rappaz M, Boettinger WJ (1999) Acta Mater 47:3205
8. Han Q, Hu H, Zhong X (1997) Metall Mater Trans 28B:1185
9. Zhang RJ, He Z, Wang XY, Jie WQ (2004) J Mater Sci 43:2072
10. El-Bealy M, Thomas BG (1996) Metall Mater Trans 27B:689
11. Miettinen J (1999) Report TKK-MK-78, Helsinki University of Technology Publications in Materials Science and Metallurgy, TKK, Espoo
12. Won YM, Thomas BG (2001) Metall Mater Trans 32A:1755
13. Cabrera-Marrero JM, Carreno-Galindo V, Morales RD, Chavez-Alcala F (1998) ISIJ Int 38:812
14. Reiter J, Bernhard C, Presslinger H (2007) Mater Charact 59:737
15. Zhang J, Singer RF (2004) Metall Mater Trans 35A:939
16. Michelic S (2004) Bacc. Thesis, University of Leoben
17. Miettinen J (1992) Metall Mater Trans 23A:1155
18. Ueshima Y, Mizoguchi S, Matsumiya T, Kajioka H (1986) Metall Mater Trans 17B:845
19. Weisgerber B, Hecht M, Harste K (1999) Steel Res 70:403
20. Cornelissen MCM (1986) Ironmak Steelmak 13:204
21. Miettinen J (2000) Metall Mater Trans 31B:365
22. Kurz W, Fisher DJ (1998) Fundamentals of solidification. Trans Tech Publications, Switzerland, Germany, UK, USA